

Université de Tunis El Manar



المدرسة الوطنية للمهندسين بتونس

école nationale d'ingénieurs de Tunis

Civil Engineering Département

## Projet de Fin d'Etudes

Realized by

**Donia Marzougui**

To obtain the

**National Engineering Degree**

in

**Civil Engineering**

# **Hydromechanical modeling of the transport and deformation in bed load sediment with discrete elements and finite volume**

**June 2011**

Subject proposed by : 3S-R lab (Grenoble INP)

Project advisors :

Bruno Chareyre : associate professor, Grenoble INP.

Julien Chauchat : associate professor, Grenoble INP.

Emmanuele Catalano : PhD student, Grenoble INP.

Examiner at home university:

Hédi Hassis: Professor, ENIT.



## *Thanks*

This report is a synthesis of four-month internship performed in the laboratory 3S-R.

The achievement of this work was made possible thanks to Mr Hédi Hassis who did not hesitate to help me in looking for research topic in France. The result is what you hold in your hands. I would like so to thank Mr Hédi Hassis, my supervisor, for the opportunity he gave me, and for the support and confidence he has shown in me.

I want to express my sincere gratitude to Bruno Chareyre, my supervisor who has always bothered to offer me the best working conditions possible. I thank him for his wide availability, his high scientific qualifications and the confidence he has shown and still shows to me today.

I express my appreciation and gratitude to Emmanuele Catalano, a PhD student in the 3s-R laboratory, for the time he spent with me, his availability even when he was abroad and the valuable advice he has given me throughout my intership.

I am also grateful to Julien Chauchat, my co-supervisor for his kindness, support and the knowledge he provided me.

A big thank you to all the students who accompanied me during these months and have continued to create a good working atmosphere within the laboratory.

I do not forget of course to send my deepest thanks to my dear parents to whom I owe so much. I would have neither the means nor the strength to accomplish this work without them.

I also want to express my gratitude to my friends who have continued to give me the moral and intellectual support throughout my work during all the good and bad moments.

They always say the best is for the end, that's why I dedicate this project to my dear twin sister Sonia, my little light that gave me energy and courage. I pray God to be with her throughout her studies of medicine. Thanks to be here!

I cannot finish these acknowledgments without paying tribute to my grandmother that I have not had the chance to see her for the last time, she unfortunately did not survive to witness this memorable moment. God bless her.

## *Contents*

General introduction.....	10
Presentation of the laboratories .....	12
1.1. Introduction .....	15
1.2. Definitions.....	15
1.2.1. Granular material.....	15
1.2.2. Fluid mechanics .....	16
1.2.2.1. Poiseuille flow.....	16
1.2.2.2. Couette flow .....	17
1.3. Rheology of dense granular flows.....	18
1.3.1. Dry granular flows.....	18
1.3.2. Immersed granular flow .....	20
1.4. Discrete element method (DEM).....	21
1.4.1. Definition and principle of the DEM .....	21
1.4.2. Computing cycle .....	22
1.4.3. Laws of motion .....	23
1.4.4. Contact laws.....	23
1.4.4.1. Stiffness model .....	24
1.4.4.2. Slip model.....	24
1.4.4.3. Convergence conditions.....	24
1.5. Software:.....	25
1.6. Conclusion:.....	26
2.1. Introduction .....	28
2.2. Different methods for the study of the solid fluid coupling .....	28
2.3. Deformable pore-network modeling .....	29
2.3.1. Volume decomposition using regular Delaunay triangulation .....	29
2.3.2. Governing equations.....	31
2.3.2.1. Continuity.....	31
2.3.2.2. Local conductance .....	32
2.3.2.3. Forces on particles .....	33
2.4. Conclusion.....	35
3.1. Introduction .....	37
3.2. Modeling of Poiseuille flow.....	37

3.3.	Fixing the computation of “A” area .....	38
3.4.	Definition of Poiseuille flow rate .....	40
3.5.	Parametric study.....	41
3.5.1.	Flow and number of grains .....	41
3.5.2.	Flow and porosity .....	41
3.5.3.	Computation of the fluid forces on particles.....	42
3.5.4.	Comparison with the analytical results.....	43
3.5.5.	Poiseuille flow for a disordered arrangement of partides.....	45
3.6.	Conclusion.....	47
4.1.	Introduction:.....	49
4.2.	Viscous shear force formulation and implementation.....	49
4.2.1.	Shear stress expression .....	49
4.2.2.	Determination of the interaction surface .....	50
4.3.	Validation for a two sphere model .....	52
4.4.	Application to a bed sediment subjected to a shearing flow.....	54
4.4.1.	Shields number.....	54
4.4.2.	Evaluation of the critical Shields number.....	55
4.5.	Conclusion.....	57
	Conclusions and perspectives .....	58
	References.....	60

## List of figures

Figure 1.1: Poiseuille flow .....	16
Figure 1.2: Shear plane (source: Andreotti et al (2011)). .....	18
Figure 1.3: (a) classification of the flow regimes as functions of I, (b) evolution of the contact network as a function of I for a shear plane obtained by a 2D numerical simulation, lines represent normal forces between particles (source Andreotti et al (2011)). .....	19
Figure 1.4: Shear plane in an immersed granular material (source Andreotti et al (2011)).....	20
Figure 1.5: diagram of the different regimes as a function of (St, r) for an immersed granular material (source Andreotti et al (2011)). .....	21
Figure 1.6: Computation cycle in the DEM .....	22
Figure 2.7: Regular Delaunay triangulation (a) and Voronoi diagrams (b). .....	29
Figure 2.8: Orientation of a cell. ....	30
Figure 2.9: Composition of a cell. ....	30
Figure 2.10: Pressure distribution on $\partial\theta_{ij}$ (a) in 2D and definition of facet spheres intersection in 3D. ....	33
Figure 3.11: Poiseuille flow model. ....	37
Figure 3.12: Delaunay triangulation problem. ....	38
Figure 3.13: Distribution of areas to compute. ....	39
Figure 3.14: S0 computation. ....	39
Figure 3.15: Q darcy and Q Poiseuille as functions of e. ....	40
Figure 3.16: $Q=f(e)$ for various number of spheres. ....	41
Figure 3.17: $Q=f(e)$ for different friction angles. ....	42
Figure 3.18: Fluid forces on particles in the right and left side of the trench as functions of e. ....	43
Figure 3.19: model of a regular mesh. ....	44
Figure 3.20: $Q/Q^* = f(e/L)$ for the different Poiseuille flows. ....	45
Figure 3.21: : Poiseuille model with irregular surface in contact with the trench. ....	46
Figure 3.22: Numerical and analytical flows as functions of e. ....	46
Figure 3.23: Voronoi diagram at the trench. ....	47
Figure 4.24: pore volume and solid area of spheres. ....	50
Figure 4.25: Interaction surface in three dimensions. ....	51
Figure 3.26: interaction surface S. ....	51

Figure 3.27: the scheme of a two sphere model ..... 52

Figure 4.28: a bed load sediment model..... 54

Figure 4.29: Distribution of the Shields number corresponding to the onset of the grain motion..... 56

Figure 4.30: Evolution of kinetic energy as a function of viscous force..... 56

## *List of tables*

Table 1: Interaction surface for the different edges: .....	52
Table 2: Shearing viscous force for a two spheres model:.....	53

*"To see a world in grain of sand,  
And a heaven in a wild flower;  
Hold infinity in the palm of your hand;  
And eternity in an hour."*

*William Blake*

## *General introduction*

During the last years, the flow of granular material in presence of interstitial fluid have been the subject of considerable researches combining inherent difficulties in granular material and those within the world of suspensions. Particles flowing in fluid undergo both contact interactions and hydrodynamic interactions. A lot of questions on the rheology of immersed granular flows are still pending.

When the granular material is strongly agitated, it behaves as a dissipative gas. At slow deformations, the quasi-static regime is described with plasticity theories. Between the two regimes, the material flows like a liquid. Many experiments have been interested in characterizing dense granular flows in different configurations; we focus our study in this project in controlling the behavior of immersed granular flows in a laminar flow.

In the last few years, new numerical methods have been proposed. They are based on discrete elements considering the soil as a discontinuous medium composed of grains in interaction. This method allowed us to study the behavior of particles assembly subjected to a shearing movement.

The present work is divided into four chapters:

Chapter 1 is devoted to the bibliography in which the most important bases of our project are introduced. First we define granular materials and the two classical flows of the fluid mechanics. Then, we talk about the rheology of granular flows. Finally, we present the Discrete Element Method (DEM), its principle, the contact laws and the computation cycle of a simulation in this method.

Chapter 2 is dedicated to introducing the solid fluid coupling model developed by E.Catalano, a PhD student in the 3S-R Lab. It aims to calculate the viscous forces exerted on the solid phase of particles.

Chapter 3 presents the study results of an immersed granular material subjected to a Poiseuille flow. The purpose of this chapter is to compare and validate the simulated Poiseuille flow with respect to theoretical Poiseuille flow.

Chapter 4 is devoted to the study of the shear in a granular material. A first part deals with the implementation of a viscous force model for sheared particles. A second one is an application to the determination of critical Shields number of immersed granular material under shearing flow.

## ***Presentation of the laboratories***

- ***Soil, Solid, Structures and Risk Lab:***

The laboratory Soils, Solids, Structures – Risks, includes all the manpower in Grenoble University on geomechanics, civil engineering and associated risks as well as mechanical and multi physics coupling in solid media complex. It is a joint research unit (UMR 5521) between CNRS (ST2I departments and EDD), the University Joseph Fourier and the “Institut National Polytechnique de Grenoble”.

The aims of the lab include analysis and development of tools for optimization and the vulnerability of structures and systems, in the field of environmental and technological risks and in the field of mechanical behavior and conduct in-service. Researches in all these domains are based on experiments developing new models which take into account the physical-mechanical coupling and multi-scale analysis, therefore is equipped with original and relevant experimental methods in mechanics of materials, geomaterials (soils, rocks, concrete) and structures. Numerical modeling, leading to powerful tools, presents the most important aim of all researches based on numerical technology advances (finite elements, discrete elements, couplings...).

3S-R, directed by Mr Jacques Desrues, receives each year about fifty doctoral students. It comprises five research teams:

- Geomaterials, Deformation and rupture (GDR): led by Pierre Bésuelle, a researcher at CNRS.
- Géomécanique et Ouvrages (GéO): led by Fabrice Emeriault, professor at “l’Ecole Nationale Supérieure pour l’Energie, l’Eau et l’Environnement » (ENSE3) in l’INP de Grenoble (INPG).
- Mécanique et couplages multiphysiques des milieux hétérogènes (CoMHet), led by Denis Favier, a professor at l’Université Joseph Fourier.
- Mécanique des matériaux solides et des milieux complexes (2MSMC) : led by Didier Imbault, an associate professor at the University of Grenoble.
- Division of risks and vulnerabilities of structures: led by Yann Malécot, a professor at University of Grenoble.
- Discrete Mechanics and Instabilities in Natural Materials (MeDiNa): led by Bruno Chareyre, an associate Professor at the University of Grenoble.

- **LEGI lab:**

LEGI, the laboratory of Geophysical and Industrial Flows, is a public research lab of the University of Grenoble. It is a joint research unit (UMR 5519) common to the national center for scientific research (CNRS), University Joseph Fourier (UJF) and Institut National Polytechnique de Grenoble (Grenoble INP) which gathers more than 180 people, including 70 permanent and as many PhD students and postdocs.

LEGI lab focuses its researches on dynamics of turbulent flows, geophysical fluid dynamics and flows with strong hydrodynamic coupling. These researches combine modeling, testing, high performance numerical simulation and the development of innovative measuring instruments. It has different resources and research facilities to conduct their projects on various aspects of fluid mechanics (aerodynamics, cavitation, rotational flow, free surface flows), both experimental (production flows) and numerical ones (modeling and simulation).

Directed by Christophe Baudet, LEGI lab comprises seven researches teams:

- EDT team: Two-Phase flows and turbulence, headed by Jean Paul Thibault a research officer.
- Energetics team, headed by Philippe Marty, a professor at Institut National Polytechnique de Grenoble.
- ERES team: Environment, Rotation and Stratification, led by Chantal Staquet a professor at Institut National Polytechnique de Grenoble.
- Houle team: Gravity Waves and Hydrodynamics Sedimentary, led by Hervé Michallet a research officer.
- MIP team: Microfluidics, interfaces, Particles, led by Jean Luc Achard, a research director.
- MEOM team: Ocean Modeling Flow Medium and Large Scale, led by Bernard Barnier.
- Most team: Modelling and Simulation of Turbulence, led by Guillaume Balarac, an associate professor at Institut National Polytechnique de Grenoble.

## *Chapter 1:*

## *Bibliography*

## ***1.1. Introduction***

The soil, a discontinuous medium, has always been assimilated and studied as a continuous medium. The use of discrete element method is one of the new approaches developing the discontinuous character of the soil. Indeed, the ground is no longer a continuous medium whose behaviour is described throughout the elementary volume, but as a set of particles interacting through contact forces. One of these methods is that of Cundall [16] which is known for its reproduction of the complexities of soil behaviour through simple laws of contact between grains.

In this chapter, we will define first the rheology of granular materials. We will then present classical flow configurations that can be encountered in the theory of immersed granular flows. Finally we will introduce the discrete element method.

## ***1.2. Definitions***

### ***1.2.1. Granular material***

We call “granular” a medium that is composed of a set of particles whose dimensions exceed 100  $\mu\text{m}$  [14]. Granular materials are found in many industrial sectors (structures and civil engineering, chemical industry, pharmaceutical industry ...) and many geophysical problems (rock avalanche, erosion, landslide, sediment transport...).

Characterization of the medium is based on the knowledge of the grain’s geometry (shape, size, ...) and mechanical characteristics (density, stiffness, ...). Interstitial fluid is likely to affect the behaviour of such material.

Studies carried out on granular materials revealed its behaviour’s complexity. Thus, according to external conditions imposed on the medium, it may have a comparable set of changes that of a solid, liquid or gas. Moreover, even in the case of apparent geometrical homogeneity, a granular packing is inherently heterogeneous in terms of mechanical stress. This property makes granular material extremely sensitive to disturbances.

A granular material has a set of pores which form a continuous network connected to the exterior medium through which a fluid can flow and modify the behaviour of the system as a whole.

## 1.2.2. Fluid mechanics

For the sake of simplicity and because flows in dense porous medium are characterized by low Reynolds number, we will consider here laminar flow problems. In what follows, we describe two classical laminar flows. The flow driven by a pressure gradient (Poiseuille flow) and the flow driven by a moving plate at a constant velocity (Couette flow).

### 1.2.2.1. Poiseuille flow

The fluid is considered Newtonian and incompressible; its volume remains constant under the action of external pressure. The fluid flows between two parallel planes whose equations are  $y= L/2$  and  $y=- L/2$  (figure 1.1) [4]. A pressure gradient is applied in the x direction between the two ends of the plans.

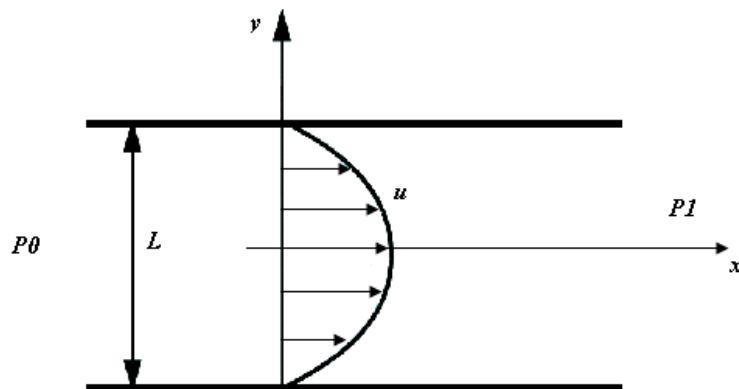


Figure1.1: Poiseuille flow

The mechanical equilibrium imposes:

$$\frac{\partial}{\partial z} \left( \eta \frac{\partial u}{\partial z} \right) + \frac{\partial p}{\partial x} = 0$$

This equation is integrated twice to give:

$$U_z = 12\eta \frac{\partial p}{\partial x} z^2 + cz + d$$

With boundary conditions:  $u(L/2) = u(-L/2) = 0$ , we get  $c=0$  and  $d= 1/2 \eta \partial p / \partial x L^2 / 4$ .

Thus velocity profile is given by the following formula:

$$U_z = 12\eta \frac{\partial p}{\partial x} \left( z^2 - \frac{L^2}{4} \right)$$

In a Poiseuille flow, velocity follows a parabolic profile with a maximum value of:

$$U_{max} = 18\eta \frac{\partial p}{\partial x} L^2$$

Flow rate is then obtained from the integral of the velocity along the z direction, and we get:

$$q = - \frac{L^3}{12\eta} \frac{\partial p}{\partial x}$$

### 1.2.2.2. Couette flow

The fluid is again Newtonian and incompressible. The fluid flows between two parallel planes whose equations are  $y=0$  and  $y=L$ , one is fixed and the other moves at a constant velocity  $U_0$  [4]. Therefore no pressure gradient exists.

The mechanical equilibrium needs:

$$\frac{\partial}{\partial z} \left( \eta \frac{\partial u}{\partial z} \right) = 0$$

We integrate this equation twice and find:

$$U_z = \frac{c}{\eta} z + d$$

Boundary conditions:  $u(0)=0$  then  $d=0$

$$u(L)=U_0 \text{ then } c=U_0 \eta / L$$

Thus the velocity profile is given by:

$$U_z = \frac{U_0 \eta}{L} z$$

In a Couette flow, the velocity profile is linear with z.

Flow rate is the integral of velocity along the direction z, and we find:

$$q = \frac{U_0 \eta L}{2}$$

### 1.3. Rheology of dense granular flows

For four decades, the scientific community has tried to understand the macroscopic behavior of flowing granular material. During the last decade, a phenomenological rheology of dense granular flows has emerged. It was shown to capture the main characteristics of such flows. Some open questions remains unanswered especially those covering localization and finite size effects.

#### 1.3.1. Dry granular flows

Let's consider the shear flow represented in the figure 1.2. A set of spherical grains (diameter  $d$  and density  $\rho_p$ ) is confined between two rough planes with a pressure  $P$  applied on the top plane moving with a velocity  $V_w$ . A velocity gradient  $\dot{\gamma} = \frac{V_w}{L}$  is imposed where  $L$  is the distance between the two planes.

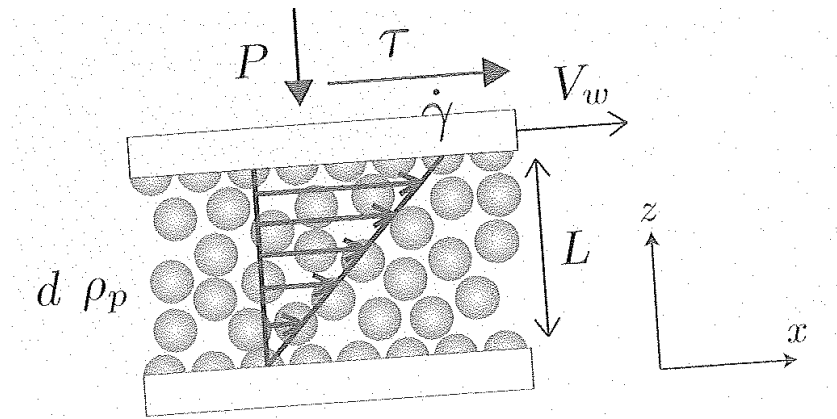


Figure 1.2: Shear plane (source: Andreotti et al (2011) [15]).

Numerical simulations using discrete element method (Da Cruz et al 2004; Iordanoff & Khonsari 2004) suggest that this system of dense granular material is controlled by a single dimensionless parameter called the inertial number [11]:

$$I = \frac{\dot{\gamma} d}{\sqrt{P/\rho}}$$

This parameter is the ratio between two time scales:

- a microscopic time scale  $d/\sqrt{P/\rho}$ : related to the confining pressure. It's the

time that a particle requires to fall in a hole of size  $d$  under a pressure  $p$ .

- a macroscopic time scale  $\frac{1}{\dot{\gamma}}$ : related to the mean shear. It's the time taken for a particle to move and reach the grain below.

Depending on this parameter's value, there are three flow regimes [12]:

- $I < 10^{-3}$ , the flow regime is quasi static (elasto-plastic material).
- $I > 10^{-1}$ , collisional regime, the material is strongly agitated.
- $10^{-1} < I < 10^{-3}$ , dense flow regime.

$I$  is the only parameter that characterizes rigid grains, the shear stress is, in fact, a function of  $I$ :

$$\tau = P\mu(I)$$

Where  $\mu$  is the effective friction coefficient.

This configuration gives then a relationship between the shear and normal stress with a friction coefficient depending on  $I$ .

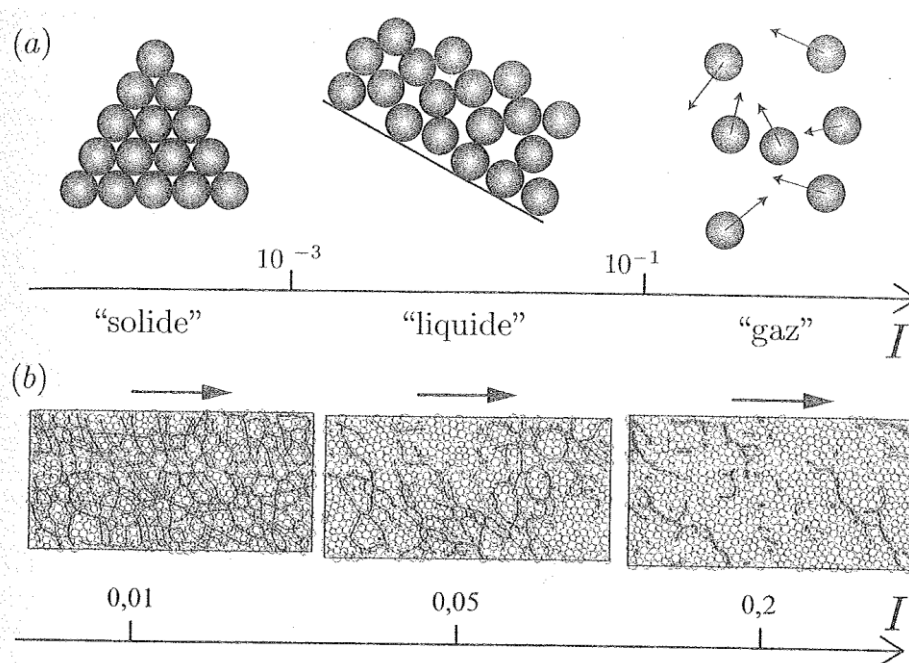


**Figure 1.3: (a) classification of the flow regimes as functions of  $I$ , (b) evolution of the contact network as a function of  $I$  for a shear plane obtained by a 2D numerical simulation, lines represent normal forces between particles (source Andreotti et al (2011)[15]).**

In order to move from quasi static to liquid and then gaseous regime, we have to increase the shear rate or decrease the confining pressure. This transition between regimes is obvious through the figure (1.3) showing the evolution of forces network as a function of  $I$ .

### 1.3.2. Immersed granular flow

Let's consider the same configuration, but this time with grains immersed in fluid of viscosity  $\eta$ . In this case, particles are confined by a normal stress  $P^p$  imposed through a porous plate allowing the fluid to flow (figure 1.4) [15]. The horizontal displacement of the plane introduces a shear  $\dot{\gamma}$ .

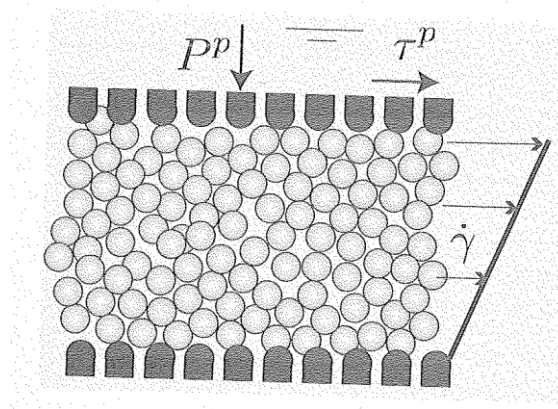


**Figure 1.4:** Shear plane in an immersed granular material (source Andreotti et al (2011) [15])

The analysis of the time  $t_{macro}$  defined for a dry flow, shows the existence of three regimes:

- Regime of free fall: the drag induced by fluid is insignificant, the regime is then the same as for dry granular flows and  $t_{micro} = d/\sqrt{P^p/\rho_p}$
- Viscous regime: the velocity of the sphere is controlled by the equilibrium between the drag force and the stress applied on the particle and  $t_{micro} = \eta/P^p$ .
- Turbulent regime: the velocity of the sphere is controlled by both the drag force and the stress applied on particles.  $t_{micro} = d/\sqrt{P^p/\rho_p C_d}$  where  $C_d$  is a drag coefficient.

The transition between these regimes is controlled by two dimensionless numbers as shown in the figure 1.5:

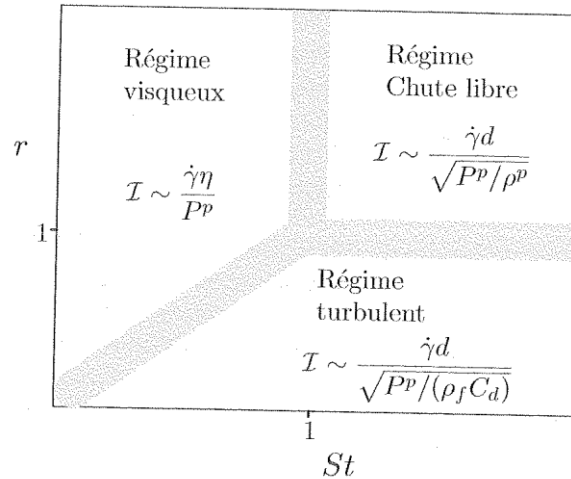


Figure 1.5: diagram of the different regimes as a function of  $(St, r)$  for an immersed granular material (source Andreotti et al (2011) [15]).

$$S_t = \frac{t_{micro}^{free\ fall}}{t_{micro}^{visc}} = \frac{d\sqrt{P^p \rho_p}}{\eta}$$

$$r = \left( \frac{t_{micro}^{free\ fall}}{t_{micro}^{turb}} \right)^2 = \frac{\rho_p}{\rho_f C_d}$$

## 1.4. Discrete element method (DEM)

### 1.4.1. Definition and principle of the DEM

The Discrete Element Method (DEM), known also as the distinct element method, is a multi-scale approach using simple interaction laws for spherical particles whose movements are governed by the fundamental principle of dynamics [1]. Proposed by Cundall in 1971, it becomes the most widely used method for solving problems of discontinuous granular materials, especially in granular flows and soil mechanics [5]. The behaviour of materials in the DEM is governed by the contact laws between materials.

The DEM simulation consists in:

- detecting collision between particles, creating new interactions and determining their properties for two particles that can be interacted.
- evaluating deformation, calculating the stresses and forces applied on particles for

already existing Interactions [2].

Detailed derivations and implementations may be found in [2].

### 1.4.2. Computing cycle

The computation cycle in the DEM is mainly characterised by two stages [6]: the first step deals with the calculation of particles' positions, the second one is about contact forces. Another step may be added, consisting on updating the list of contacts.

In fact, a list of current contacts is required to determine the shape, the position and the orientation of particles. The procedures in place for that purpose can save time by elaborating or making a list of potential contacts based on the division of the space with a grid, so that, two particles are in contact if the distance between their centres is inferior to the sum of their radii.

The normal and shear contact forces, are calculated separately, with the use of the interaction law. We then deduce the torque effort applied on each particle.

The next step concerns the kinematic evolution of grains according to the law of motion which will be presented in the following paragraph.

The computation cycle in the DEM is shown schematically in the figure 1.6:

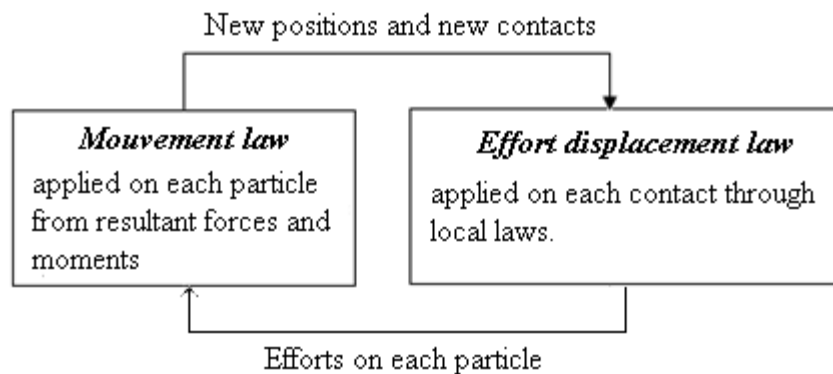


Figure 1.6: Computation cycle in the DEM [6]

### 1.4.3. Laws of motion

The granular material is represented by a stack of spherical particles. Each one is characterised at time  $t$  by its position  $y_i$ , linear velocity  $\dot{y}_i$  and angular velocity  $\dot{w}_i$ . Knowing the positions of particles, we can find at any time a list of contacts for each particle and then calculate the interaction forces between particles.

If we denote  $m_p$  the mass of a particle and  $I_p$  its inertia, we can determine the acceleration in translation and rotation according to the principle of dynamics [5]:

$$\ddot{y}_i = \frac{F}{m_p}$$

$$\ddot{w}_i = \frac{M}{I_p}$$

Where  $\{F, M\}$  is the resultant torque of contact forces on particle.

Grains are moving during the simulation, so we denote their positions at each time step  $\Delta t$ .

We suppose that accelerations have already been calculated by successive integrations along a centered finite difference scheme on a time step  $\Delta t$ , we obtain velocities at  $t + \Delta t/2$  :

$$[\dot{y}_i]_{t+\Delta t/2} = [y_i]_{t-\Delta t/2} + [\dot{y}_i]_t * \Delta t$$

$$[\dot{w}_i]_{t+\Delta t/2} = [w_i]_{t-\Delta t/2} + [\dot{w}_i]_t * \Delta t$$

The new positions of particles at  $t + \Delta t$  are:

$$[y_i]_{t+\Delta t} = [y_i]_t + [\dot{y}_i]_{t+\Delta t/2} * \Delta t$$

$$[w_i]_{t+\Delta t} = [w_i]_t + [\dot{w}_i]_{t+\Delta t/2} * \Delta t$$

Contact forces are recalculated taking into account the new positions of particles.

All these interactions are performed to converge the system towards a state of static equilibrium.

### 1.4.4. Contact laws

The contribution of the DEM is its ability to reproduce complex mechanical phenomena while retaining a small number of mechanical parameters. To achieve this goal, it is necessary to implement simple laws of interactions:

#### 1.4.4.1. Stiffness model

This model provides an elastic relationship between the contact force and the relative displacement.

The contact laws between particles connected by springs are characterized by a normal stiffness  $K_n$  and a shear stiffness  $k_s$ .

Among the various types of contact laws, we can mention that of Hertz-Mindlin [9] which is a non-linear contact formulation reflecting the deformation between two elastic spheres depending on the shear modulus  $G$  and the Poisson coefficient  $\nu$ . This type of contact is complicated enough, that's why we choose the laws of constant stiffness.

The normal contact force is:  $F_i^n = K^n U^n$

The increment of shear contact force is:  $\Delta F_i^s = k^s \Delta U_i^s$

Where  $U^n$  and  $\Delta u_i^s$  are respectively the total normal displacement and the increment of shear displacement.

#### 1.4.4.2. Slip model

The slip model enforces a relation between normal and shear contact forces so that the two contacting spheres can relatively slip to one another.

It allows slip to occur by limiting the shear force. Its expression is a function of the normal force:

$$|F_t| \leq F_n \tan \mu_s$$

Where  $\mu_s$  is the friction coefficient at the contact.

#### 1.4.4.3. Convergence conditions

When the grains are interacting through a spring, waves are then likely to spread. The calculation by the DEM will be stable only if the time-step is smaller than the smallest Eigen period in the system [1]. Each grain of the assembly can be compared to an oscillator of mass  $m$  connected to a fixed body by a spring of stiffness  $k$ . the period  $T$  of the oscillator can be defined by:

$$T = 2\pi \sqrt{\frac{m}{k}}$$

We must use a time step large enough to describe this oscillation. A critical time step is set automatically at the beginning of each cycle. We determine for each degree of freedom  $i$  the equivalent contact stiffness  $K_i$  surrounding the element.

$$\Delta_{crit} = S * \min \left( \sqrt{\frac{m_i}{K_i}} \right)$$

Where  $S$  is the fraction of the smallest period obtained on all particles.

The DEM provides at each calculation cycle the dynamic equilibrium of the granular assembly. The purpose is to reach a state of static equilibrium by maintaining the principle of the DEM. If the contact interactions are purely elastic, no energy is then dissipated. The computer codes allow the introduction of a damping in the grain system called viscous or non viscous.

Viscous damping is to connect each grain of the assembly by dampers working in translation and rotation. This introduces energy dissipation at the interactions between the grains in contact with shock absorbers.

Cundall has proposed a non-viscous damping that applies independently to each grain. Damping force is then proportional to the resultant force on the grain.

### ***1.5. Software:***

Different computer codes are developed for DEM simulations. Some are commercial software, like PFC [17], others are in-house codes developed in scientific institutions and a few of them are distributed under open-source licenses like the software Yade.

Yade is an extensible open-source framework for discrete numerical models, based on Discrete Element Method [2]. The project started as a result of SDEC at Grenoble University and is nowadays developed in several research units. Yade use C++ for computation and allows the implementation of new algorithms, the incorporation of interface with other programs and operations of imports and exports data. Python can also be used to create and manipulate the simulation. Details of this code can be in the appendix A.

## ***1.6. Conclusion:***

Basic knowledge required to understand this work have been presented in this chapter. The study of shear in a dense granular flow is developed according to the DEM. For that purpose, Yade will be used.

## *Chapter 2:*

### *Solid fluid coupling*

## ***2.1. Introduction***

This chapter concerns the presentation of the solid fluid coupling model [7] developed by Emmanuele Catalano, a Phd student in the 3S-R lab. His work represents the first step in the development of an efficient model for saturated granular material under stress, aiming at determining the viscous forces applied on particles. We first review briefly the existing methods for coupling discrete models with fluid flow. Next, we detail Catalano's model.

## ***2.2. Different methods for the study of the solid fluid coupling***

Various methods have been presented in the literature in order to model the solid fluid coupling. They differ in the decomposition of the pore volume.

- Microscale Stokes flow modeling: the numerical Stokes solution is reflecting in details complex three-dimensional pore geometries which uses the Finite Element Method, finite volumes, Lattice Boltzmann and other methods.
- Continuum-discrete Darcy flow modeling: this approach uses the coarse-grid CFD methods where the flow and the solid-fluid interactions are defined with simplified semi-empirical models based on Darcy law. Despite its performance in making coupled problems affordable in terms of CPU cost, this method cannot be efficient in solving some problems like segregating phenomena, internal erosion by transport of fines,...
- Pore-network modeling: this approach was developed to predict the permeability of materials from microstructural geometry using a simplified representation of porous media. It was a well-known strategy for its appropriate definition of how fluids are distributed between pores. Usually, it's used with undeformable solid skeleton.
- Deformable pore-network modeling: this approach had focused its studies in developing expressions of forces applied on solid particles in the aim to be used in three-Dimensional DEM simulations. This solution was limited to 2D models of discs assemblies, it has been adapted to 3D assemblies in the work of Catalano.

## 2.3. Deformable pore-network modeling

### 2.3.1. Volume decomposition using regular Delaunay triangulation

Delaunay triangulation (figure 2.7.a) and the Voronoi graph (figure 2.7.b) are used for structural study of molecules, liquids and granular materials. The most used Delaunay model is defined for a set of points. The graph of Voronoi defines, in this case, polyhedra around each point and facets of the polyhedra are equidistant to two adjacent points.

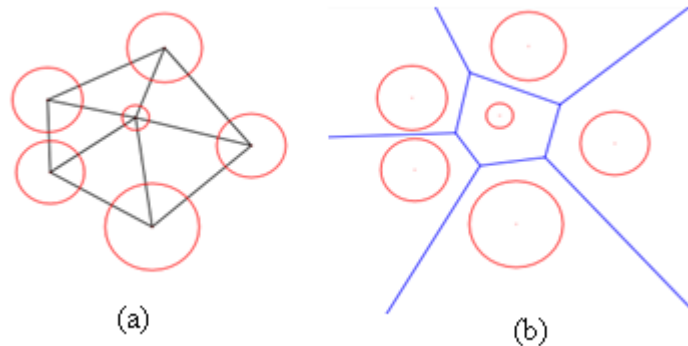


*Figure 2.7: Regular Delaunay triangulation (a) and Voronoi diagrams (b).*

The Computational Geometry Algorithms Library CGAL, an Open Source Project, is the library used to access to efficient geometric algorithms in the form of a C++ library and define the Regular Delaunay triangulation and Voronoi graph. [13].

The triangulation is a set of points called vertices and a collection of cells linked together through incidence relations.

Each cell gives access to its four incident vertices and adjacent cells. However, each vertex gives access to one of its incident cells.

The vertices of each cell are indexed with 0, 1, 2 and 3 in positive orientation, the neighbors too, such the way that the neighbor indexed by  $i$  is opposite to the vertex  $i$ .

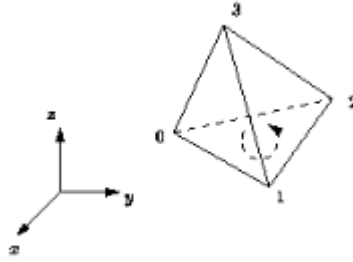


*Figure 2.8: Orientation of a cell [13].*

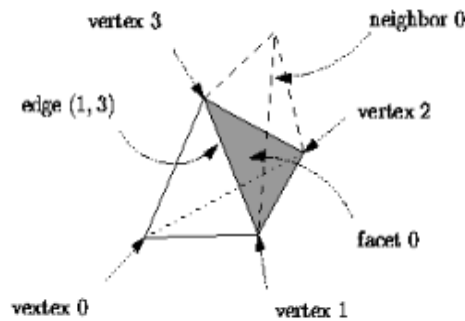


*Figure 2.9: Composition of a cell [13].*

The Voronoi cells  $S$  are often used. They define the split between the spheres as curved surfaces equidistant from both spheres surfaces. But using this type of graph is computationally costly for surfaces and volumes. To avoid this problem, regular Delaunay triangulation was then proposed. It uses weighted points where weights account for the radius of the spheres. The Voronoi graph is then entirely contained in the voids between the spheres, which is not possible for the classical Delaunay triangulation. Edges and facets of the regular Voronoi graph are lines and planes enabling a quick and easy computation of geometrical quantities.

In what follows, we will use the combination of facets of the regular Delaunay triangulation and vertices of the regular Voronoi graphs, in order to decompose the voids volume.

$\Omega$ : domain occupied by a porous material will be decomposed to:

$\Gamma$ : domain occupied by solid.

$\Theta$ : domain occupied by fluid.

$N_c$  is the number of tetrahedral cells in the regular Delaunay triangulation of the spheres packing.

$\Omega_i$  is the domain defined by the tetrahedron I.

We have:  $\Omega = \sum_1^{N_c} \Omega_i$

We define  $N_s$  as the number of spheres and  $\Gamma_i$  as the domain occupied by the sphere i.

We have  $\Gamma = \sum_1^{N_s} \Gamma_i$

### 2.3.2. Governing equations

#### 2.3.2.1. Continuity

We define  $\Theta_i$  as the part of the tetrahedron  $\Omega_i$  occupied by fluid, its volume is  $V_i^f$ .

The continuity equation of an incompressible fluid is:

$$V_i^f = \int_{\partial\theta_i} (v - u)n \, dS$$

Where  $\partial\theta_i$  the contour of the domain  $\theta_i$  and  $n$  is the outward pointing unit vector normal to  $\partial\theta_i$ .

$u$  is the fluid velocity and  $v$  is the contour velocity.

We define  $\partial^s \theta_i$  as the solid-fluid interface where we have:  $(v - u)n = 0$ . So the integration can be restricted to  $\partial^f \theta_i$ , the fluid interface.

We introduce  $S_{ij}^f$  ( $j \in (j_1, j_2, j_3, j_4)$ ) the intersections of triangular surfaces  $S_{ij}$  with the fluid domain, so that,  $\partial^f \theta_i = \sum_{j_1}^{j_4} S_{ij}^f$ , we can define the fluid flux from tetrahedron I to adjacent tetrahedra  $j_1$  to  $j_4$ :

$$V_i^f = \sum_{j_1}^{j_4} \int_{S_{ij}^f} (v - u)n \, dS = - \sum_{j_1}^{j_4} q_{ij}$$

The volume  $V_i^f$  is constant since we supposed that particles are fixed. So the continuity equation is simplified to:

$$\sum_{j=1}^{j_4} q_{ij} = 0$$

### 2.3.2.2. Local conductance

The domain  $\Omega$  is defined as a set of subdomains  $\Omega_{ij}$ , the union of two tetrahedra constructed from facet  $S_{ij}$  and Voronoi vertices  $P_i$  and  $P_j$  and  $\Theta_{ij}$  is a throat connecting two pores. Its length is  $L_{ij} = |P_i - P_j|$

$\Phi_{ij}$  is the volume of  $\Theta_{ij}$  and  $\gamma_{ij}$  is the surface of  $\partial^s \Theta_{ij}$ , the part of the contour in contact with spheres.

The hydraulic radius is defined as follows:

$$R_{ij}^h = \frac{\Phi_{ij}}{\gamma_{ij}}$$

So that we have:

$$q_{ij} = g_{ij} \frac{(p_i - p_j)}{L_{ij}}$$

$$g_{ij} = \chi \frac{A_{ij} R_{ij}^{h^2}}{\mu}$$

$g_{ij}$  is the local conductance of the facet  $ij$  and  $p_i - p_j$  is the pressure difference between two connected tetrahedral cells.

$\chi$  is a shape factor taken equal to  $2\pi$ , by analogy with the Hagen-Poiseuille law for cylindrical tubes.

### 2.3.2.3. Forces on particles

The force applied on the particle  $k$  by fluid is decomposed in two terms:

- $F^{p,k}$ , the pressure stress on the contour  $\partial\Gamma_{ij}$ .
- $F^{v,k}$ , the viscous stress on the contour  $\partial\Gamma_{ij}$ .

$$F^k = \int_{\partial\Gamma_{ij}} (pn + \tau n) dS = \int_{\partial\Gamma_{ij}} pn dS + \int_{\partial\Gamma_{ij}} \tau n dS = F^{p,k} + F^{v,k}$$

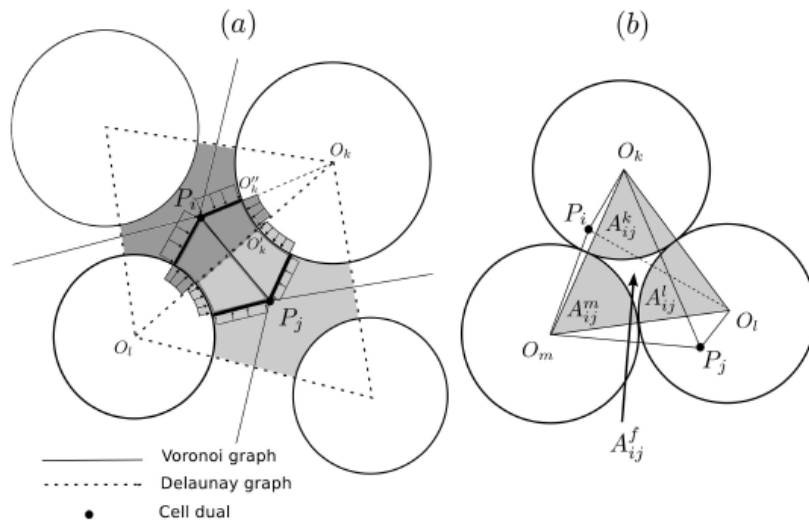


Figure 2.10: Pressure distribution on  $\partial\theta_{ij}$  (a) in 2D and definition of facet spheres intersection in 3D. [7]

- **Pressure stress**

The force generated by pressure on particle  $k$  in the domain  $\Omega_{ij}$  is the sum of two terms  $p_i$  and  $p_j$ .

$$F_{ij}^{p,k} = \int_{\partial\Gamma_{ij} \cap \partial\Omega_{ij}} p_i n dS + \int_{\partial\Gamma_{ij} \cap \partial\Omega_{ij}} p_j n dS$$

In the domain  $\Omega_{ij}$ , the pressure stress is proportional to the area  $A_{ij}^k = S_{ij} \cap \Gamma_k$ . Noting that  $n_{ij}$  is the unit vector pointing from  $P_i$  to  $P_j$ , the pressure force is then:

$$F_{ij}^{p,k} = A_{ij}^k (p_i - p_j) n_{ij}$$

- *Viscous stress*

The integration of the total viscous stress applied on the solid phase in  $\Omega_{ij}$  gives a total viscous force:

$$F_{ij}^v = \int_{\partial\theta_{ij}^s} \tau n \, dS$$

Using the divergence theorem, we obtain:

$$\int_{\partial\theta_{ij}} (pn + \tau n) \, dS = 0$$

Or:

$$\int_{\partial^s \theta_{ij}} \tau n \, dS + \int_{\partial^f \theta_{ij}} \tau n \, dS + \int_{\partial\theta_{ij}} pn \, dS = 0$$

If we suppose that pressure gradients are equilibrated by viscous stress on the solid phase only, thus neglecting the term  $\int_{\partial^f \theta_{ij}} \tau n \, dS$  gives:

$$F_{ij}^v = - \int_{\partial\theta_{ij}} pn \, dS = A_{ij}^f (p_i - p_j) n_{ij}$$

In order to express the viscous force applied on each of the three spheres in  $\Theta_{ij}$ , we consider that the force on a sphere is proportional to the surface of the sphere contained in the subdomain. Then:

$$F_{ij}^{v,k} = F_{ij}^v \frac{\mathcal{V}_{ij}^k}{\sum_1^3 \mathcal{V}_{ij}^k}$$

## ***2.4. Conclusion***

We have defined in this part of the report the viscous force applied on the solid phase of particles by means of the regular Delaunay triangulation.

These forces were determined by neglecting the viscous stress applied on fluid-fluid parts of the interfaces between volume elements. As a consequence, the model can't give correct estimates of viscous forces generated by shear deformation. This will be one of the inputs of the present work.

## *Chapter 3:*

### *Poiseuille flow test case*

### 3.1. Introduction

In this chapter the response of the model in a Poiseuille-like configuration will be studied. The numerical model generated by Yade represents a packing of spheres in which is entailed a Poiseuille flow. The results will be compared with the analytical solutions in order to validate our computational model.

Two types of interactions are present in this model: sphere- sphere interaction and fluid- sphere interaction. We are interested in our study in controlling grains' behavior in presence of fluid and calculating forces generated on particles.

### 3.2. Modeling of Poiseuille flow

Let us consider a cubic box with dimensions  $(0.2*L*L)$  containing spheres with a dispersion of radii of 1%. We translate this block of spheres with a distance  $e$  (m) along the  $x$  axis, so we get two symmetric blocks from the plane of equation  $x = 0.2 + e/2$ . We impose a pressure gradient equal to 1 and we choose a value of  $L = 1$  m.

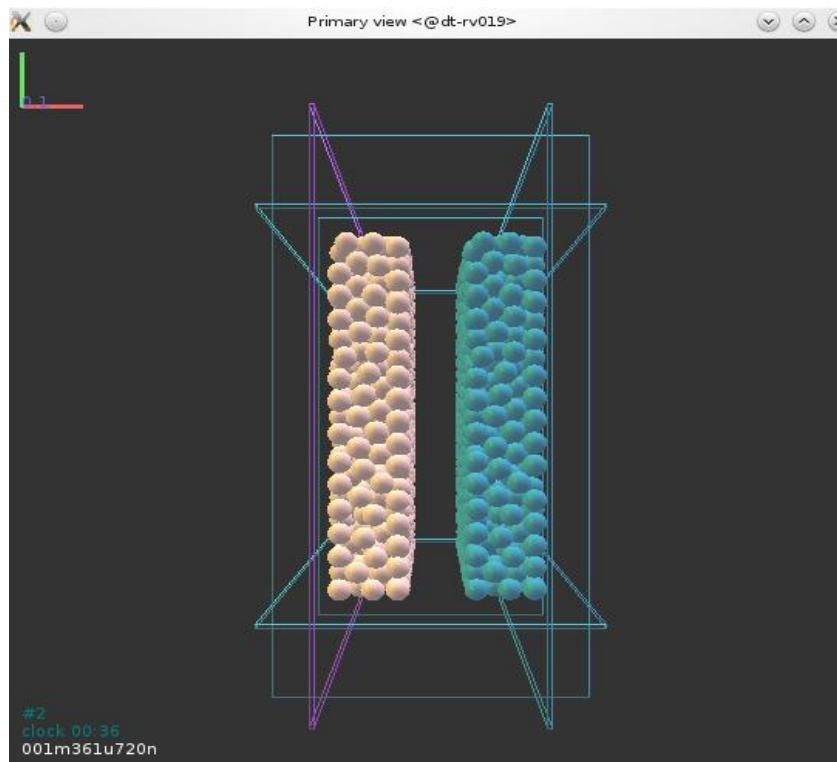


*Figure 3.11: Poiseuille flow model.*

We recall that, by analogy with the Poiseuille's formula for a cylindrical tube, we define a parameter called the hydraulic conductance as:

$$g = \frac{R_h^2 A}{\chi \eta}$$

Where  $R_h$  is the hydraulic radii,  $A$  is the fluid area,  $\chi$  is the shape coefficient and  $\eta$  is the viscosity.

The expression of the flow rate is then:

$$Q = g \frac{\Delta p}{\Delta z}$$

### 3.3. Fixing the computation of “A” area

By performing the computation of the flow rate, we initially found unexpected discrepancies in results; there are areas that give us infinite values of permeability and flow rate. Careful review of the code revealed that it was due to a special case in the decomposition of the volume by the method of Delaunay triangulation that was not treated correctly in the original code. We detail here how we find this problem.

Obtained triangles linking, as was already mentioned, the centers of the spheres, at most, one facet of each triangle could cut the solid surface of a sphere belonging to the same triangle (figure 3.11). The surface of the triangle would be smaller than the sum of solid surfaces in contact with the fluid, giving consequently a negative value of the fluid surface, which is physically impossible.

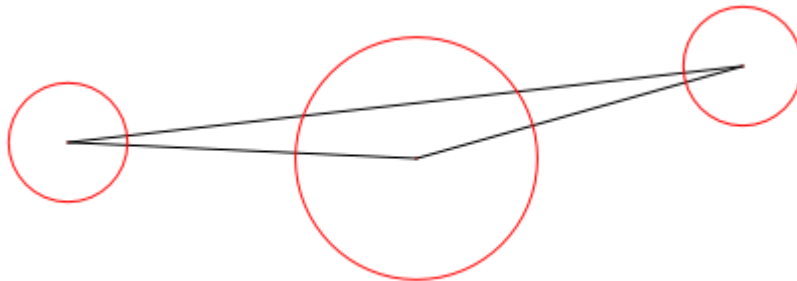


*Figure 3.12: Delaunay triangulation problem.*

To overcome this problem, we must take into account the solid surface that does not belong to the triangle on which we make the computation of permeability.

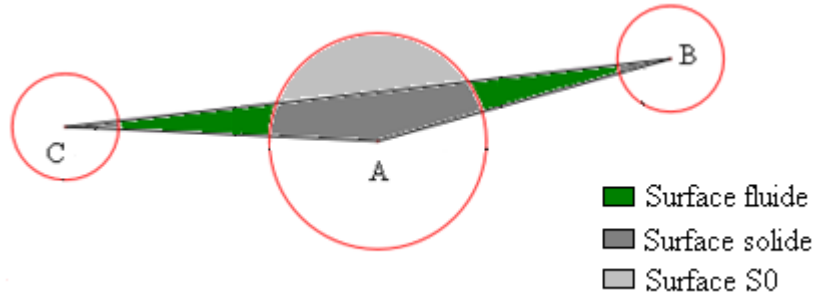


Figure 3.13: Distribution of areas to compute.

We calculate the surface  $S_0$ , the part of the sphere that doesn't belong to the triangle and would be subtracted from the calculation of the fluid area.

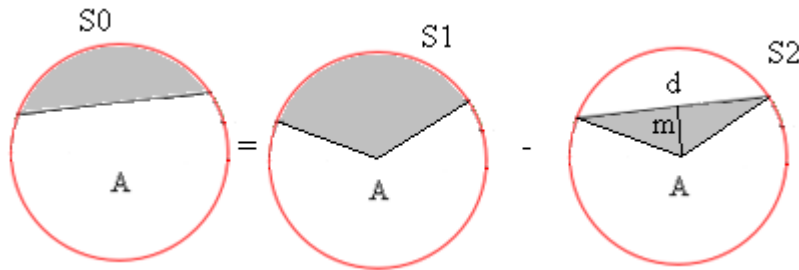


Figure 3.14:  $S_0$  computation.

$$S_0 = S_1 - S_2$$

$$S_1 = 0.5 R^2 \theta$$

$$S_2 = 0.5 m d$$

Where:

$$m = \frac{\|\vec{BA} \wedge \vec{BC}\|}{\|\vec{BC}\|} \text{ the distance of the sphere A from the opposite facet BC.}$$

$$d = 2 \sqrt{R_0^2 - m^2}$$

$$\theta = 2 \cos^{-1} \frac{m}{R_0}$$

### 3.4. Definition of Poiseuille flow rate

Once the fluid area is correctly computed, we can calculate the flow which is actually the sum of two flows: the Poiseuille flow generated through the trench (zone between the two blocks of spheres separated by the gap  $e$ ) and the Darcy flow through the pores between grains:

$$Q = 2Q_{Darcy} + Q_{Poiseuille}$$

$$Q_{darcy} = KA' \frac{\Delta p}{\Delta z}$$

Where  $k$  is the permeability which corresponds to  $e = 0$ .

$$A' = 0.2 * L$$

For a packing of 20 000 spheres, we have calculated the average Poiseuille flow for different values of  $e$  (figure 3.5).

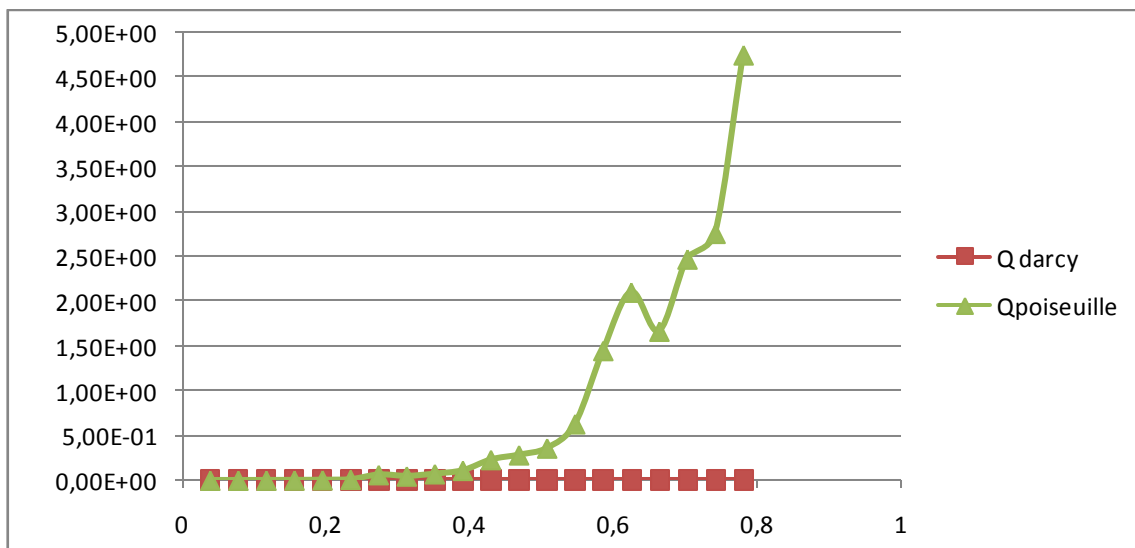


Figure 3.15:  $Q_{darcy}$  and  $Q_{Poiseuille}$  as functions of  $e$ .

As we can see, the Darcy flow is very small, negligible compared to Poiseuille flow. This can be explained by the difference of permeabilities which is a function of area (pore's area is very small compared to the trench's one).

We can then consider that the flow rate generated by Yade is approximately equal to the Poiseuille flow rate.

### 3.5. Parametric study

We study here the properties of the numerical flow rate for the already described model with a smooth plane surface in contact with the fluid in the trench in order to be comparable with the theoretical plane Poiseuille. We will show at the end the difference in terms of the flow rate between considering a smooth and a rough surface by presenting some obtained results.

#### 3.5.1. Flow and number of grains

In this section, we will calculate the flow rate through this configuration as a function of  $e$  for various numbers of spheres.

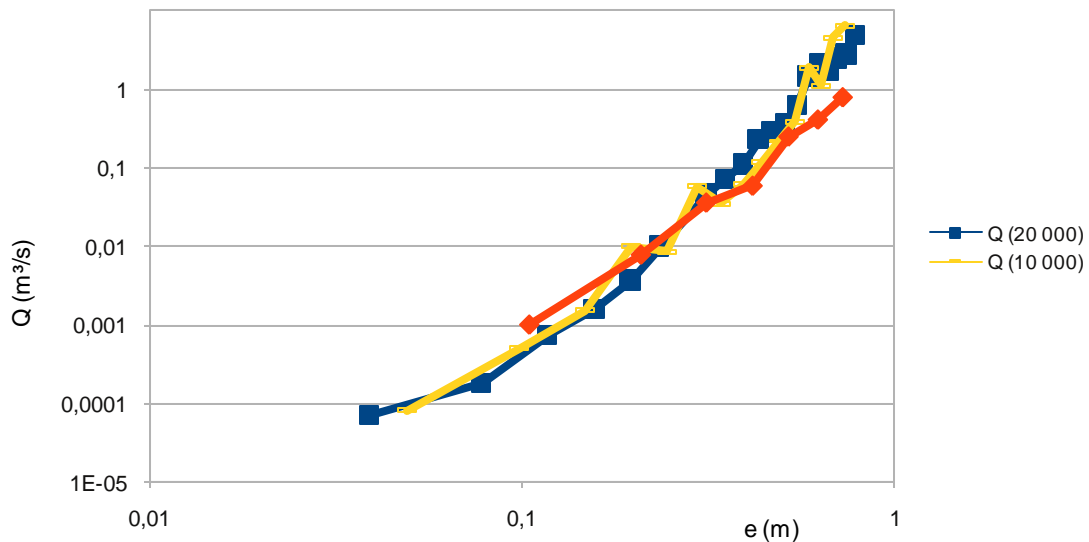


Figure 3.16:  $Q=f(e)$  for various number of spheres.

In figure 3.15, we have presented the variation of the flow rate as a function of the trench's width for various number of spheres (from 1 000 to 100 000 spheres). We can clearly see that the curves  $Q=f(e)$  are very close one to the other. We can conclude then that the flow is independent from the number of spheres.

#### 3.5.2. Flow and porosity

In this section, we are interested in the influence of porosity which is controlled by the friction angle defined as an intrinsic characteristic of the material. Figure 3.16 shows the comparison

of flow rate versus gap width for two values of porosity. The smaller the porosity is the denser is the granular assemblage.

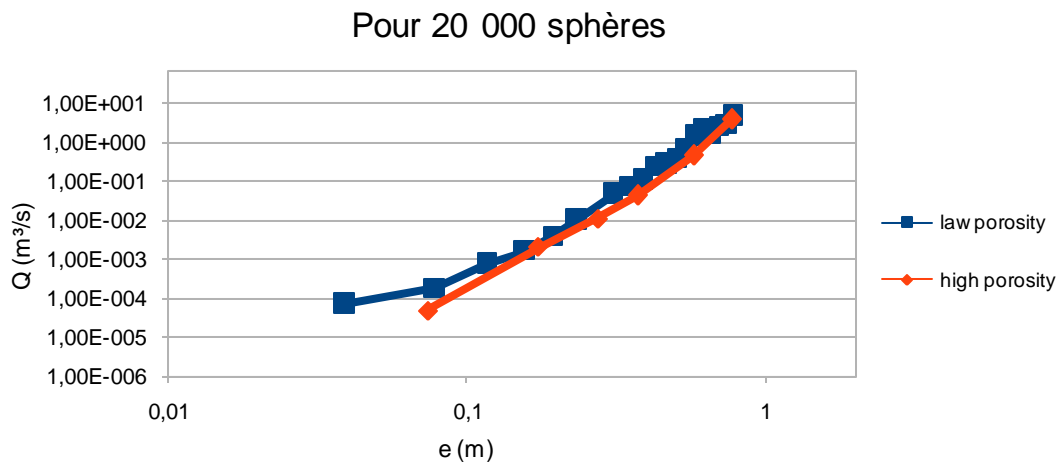


Figure 3.17:  $Q=f(e)$  for different friction angles.

We see that the flow rate for  $\varphi = 0$  have slightly increased. Indeed, the material is denser, the pores' volume is reduced and the permeability decreases. Consequently, the Darcy flow decreases and the reduced amount is added to the Poiseuille flow since the incoming flow is equal to the outgoing flow.

The two curves are very close to each other, the flow rate is independent from the porosity.

### 3.5.3. Computation of the fluid forces on particles

In this section, we calculate the forces generated by the fluid on the first layer of spheres in contact with the trench.

In one hand, we calculate the force applied on the left side of the trench and in the other hand the force applied on the right side of the trench, as a function of the trench's width.

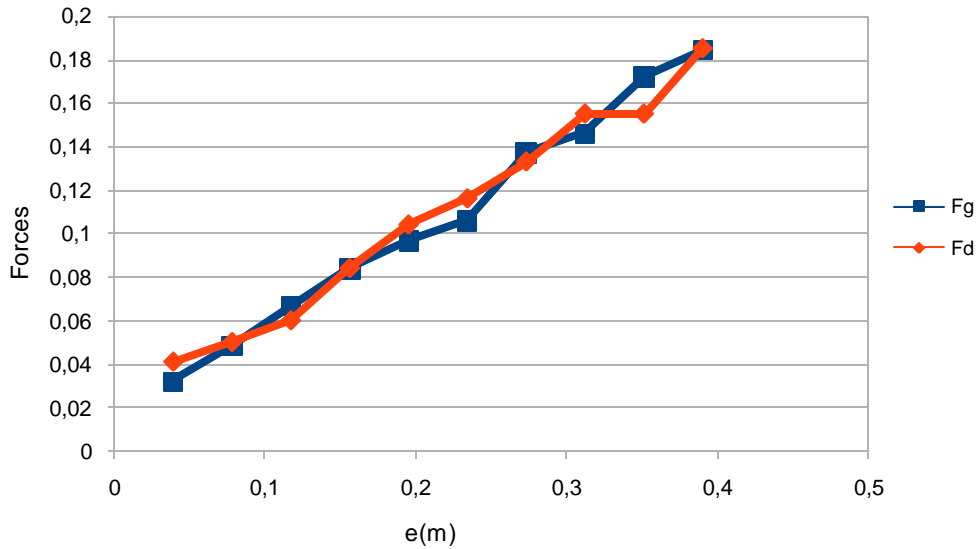


Figure 3.18: Fluid forces on particles in the right and left side of the trench as functions of  $e$ .

We consequently notice that the two curves coincide; the values of the right force and the left one are almost the same. It confirms that our problem is symmetric.

Results are represented in this graph by the norms of fluid forces. The value of the  $x$  component is very insignificant compared to the  $y$  component which represents in other terms the viscous force.

The curve of the viscous force as a function of the gap  $e$  is linear. In fact, we have:

$$F_v = - \int p dS = A_f (p_0 - p_1)$$

Where  $A_f = e * L$  is the fluid area.

$$\text{So } F_v = eL(p_0 - p_1)$$

Since  $(p_0 - p_1) = 1$  and  $L = 1$ ;  $F_v = e$

This result is additionally proving what we have obtained by Yade.

### 3.5.4. Comparison with the analytical results

The flow obtained by Yade will be compared to three analytical solutions of Poiseuille flow.

The first is the Poiseuille flow between two parallel planes given by:

$$Q = \frac{e^3 \Delta p}{12n \Delta z}$$

The second one is the same as defined above but taking into account the radius of spheres on

both sides of the trench. This means that:

$$Q = \frac{h^3 \Delta p}{12n \Delta z}$$

Where  $h = e + 2r$ .

The third one is that calculated for a regular mesh as shown in figure 3.18:

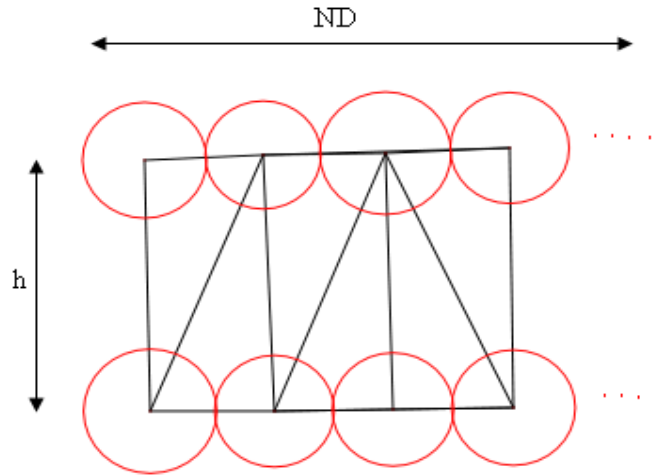


*Figure 3.19: model of a regular mesh.*

Let's calculate the permeability  $K$  for one cell.

$$K = \frac{A_f R_h^2}{2\eta}$$

$$R_h = \frac{V_v}{S_s} = \frac{h(2r)^2 - 4/3\pi r^3}{2\pi r^2} = \frac{h}{\pi} - \frac{r}{3}$$

$$A_f = rh - \frac{\pi r^2}{2}$$

The flow rate generated by the model is then:

$$Q_T = 2N K \frac{\Delta P}{ND}$$

Figure 3.19 shows the evolution of  $Q/Q^* = f(e/L)$  where  $Q$  is the flow rate and  $Q^*$  is:

$$Q^* = \Delta p L^3 / \eta$$

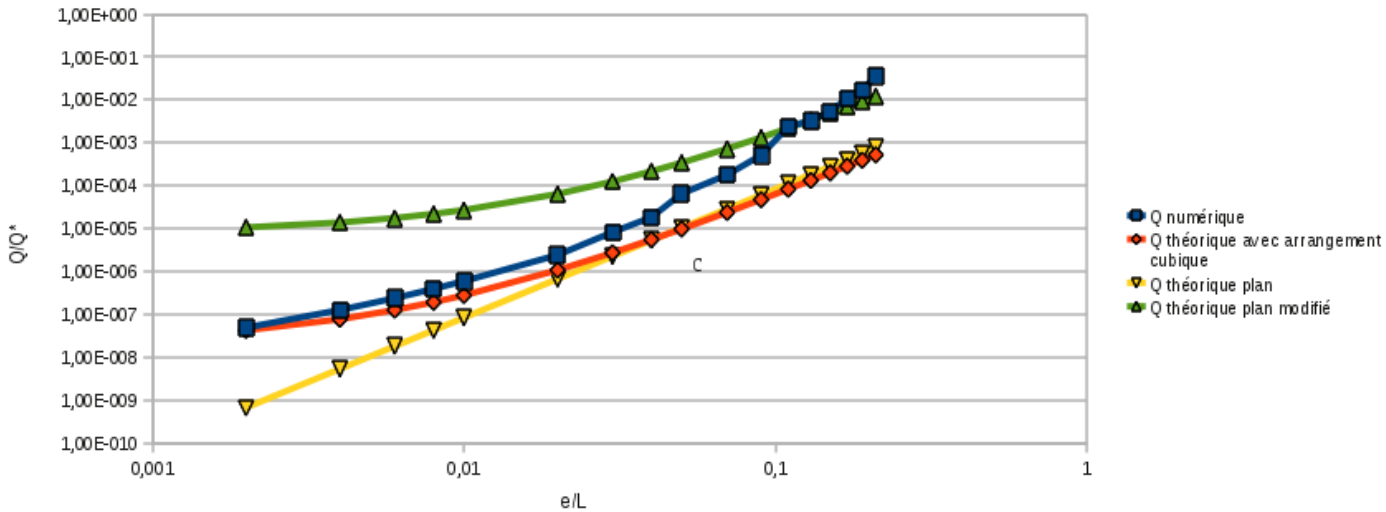


Figure 3.20:  $Q/Q^* = f(e/L)$  for the different Poiseuille flows.

We notice that for small values of  $e$ , the asymptotic behavior result of the numerical flow rate is close to the regular Poiseuille one. For large values of  $e$ , the numerical flow rate diverges from the regular Poiseuille solution because particles are no longer seen by the fluid in the trench in terms of Voronoi graphs.

The two curves for plane Poiseuille  $Q = f(e)$  and  $Q = f(h)$  coincide for large values of  $e$ . This can be explained by the fact that the larger the gap width is, the more the radius  $r$  is negligible and the more  $h$  approaches to  $e$ .

### 3.5.5. Poiseuille flow for a disordered arrangement of particles

Let's consider a cubic box with dimensions  $(L * L * L)$  containing spheres with a dispersion of radii of 1%. We design an area  $e$  (m) wide where no sphere should exist, so that the two blocks of the spheres placed on both sides of this area play the role of two parallel planes of equations  $x = L/2$  and  $x = -L/2$ .

We impose a pressure gradient equal to 1 and we choose a value of  $L = 1$  m.

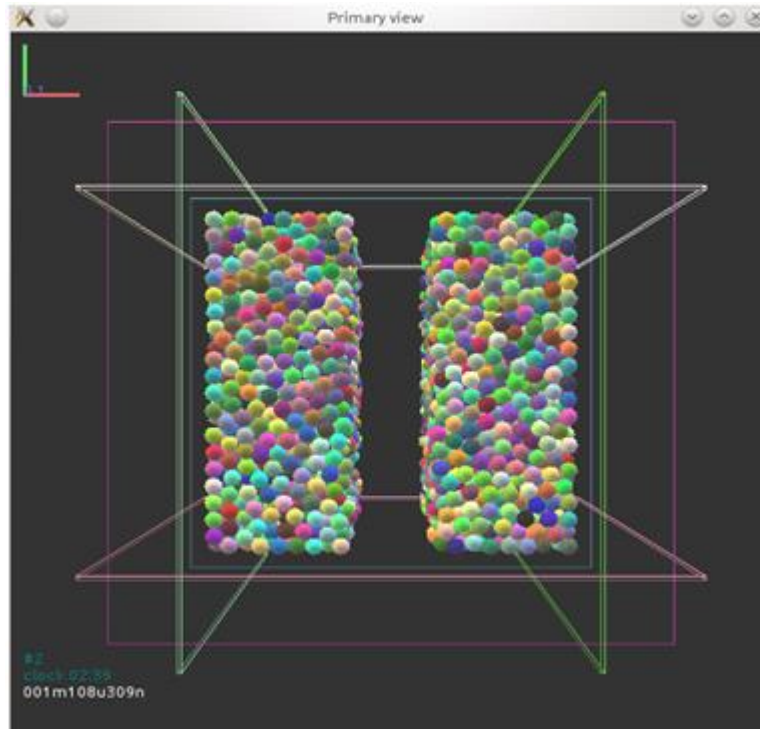


Figure 3.21: : Poiseuille model with irregular surface in contact with the trench.

We compare the flow rate generated by Yade to theoretical values of Poiseuille flow calculated from the formula below:

$$Q = \frac{e^3 \Delta p}{12n \Delta z}$$

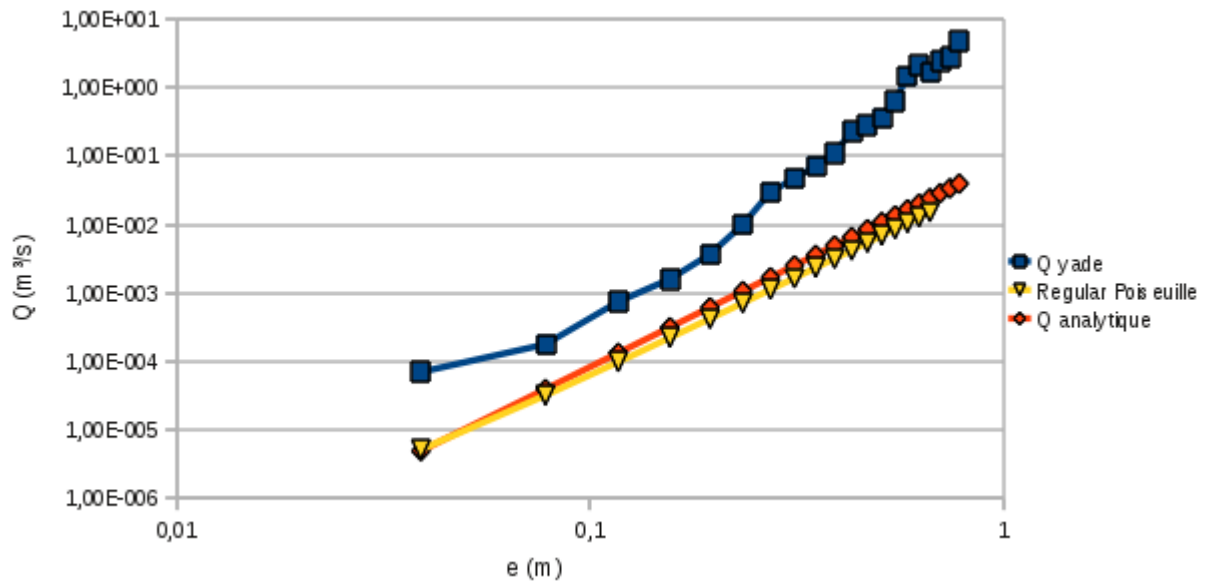
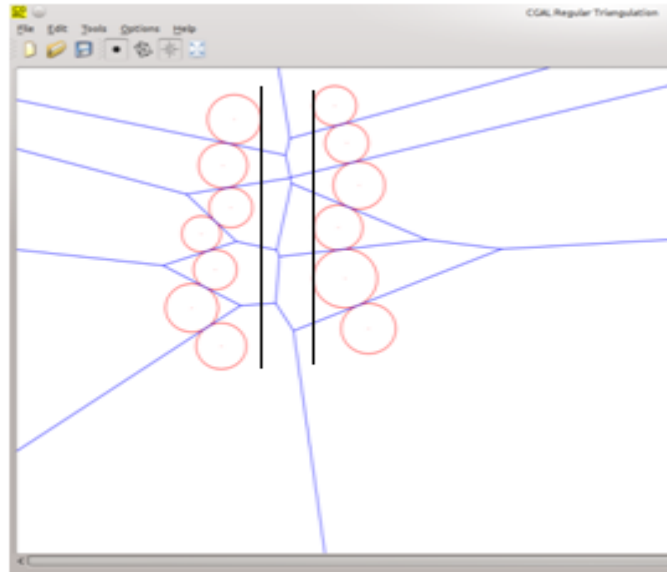


Figure 3.22: Numerical and analytical flows as functions of e.

We notice that the values of  $Q_{yade}$  are slightly larger than those of theoretical Poiseuille. Comparing  $Q_{yade}$  with the numerical flow calculated in the previous section for an idealized configuration, we find that

This is caused by the fact that the surface of all spheres in contact with fluid is not quite regular and spheres are not perfectly aligned as we can see in the graph below which shows us the Voronoi graph.



*Figure 3.23: Voronoi diagram at the trench.*

This graph shows us the Voronoi diagram (with blue lines) and the width  $e$  of the trench that has been created. We can clearly see that the fluid surface limited by Voronoi diagrams is slightly larger than that limited by the trench. So, the flow would be undoubtedly larger than the analytical flow.

### **3.6. Conclusion**

The flow rate generated by Yade is in agreement with the analytical Poiseuille flow rate. Moreover, we have checked that this flow rate is independent of the geometrical and mechanical properties of the grains.

## ***Chapter 4:***

### ***Modeling of shear in a Couette flow***

## 4.1. Introduction:

When a bed of particles is subjected to a shearing flow, the particles on the surface can be set in motion. This is linked with many problems of sediments transport and an active area of research. That's why we will be interested in this chapter in the derivation of expressions for the viscous forces generated in such case.

First, we will define the viscous shear force as functions of shear deformation at the particles scale. Next, we will simulate the evolution of bed sediment under the effect of a shearing flow and analyze the results in terms of shields number.

## 4.2. Viscous shear force formulation and implementation

The shearing viscous force is given by the formula below. It is the product of the shear stress and the surface on which this stress is applied.

$$F = \tau S$$

### 4.2.1. Shear stress expression

The shear stress is obtained from dimensional consideration as a velocity difference between two neighboring particles times the fluid viscosity, divided by a characteristic distance between the two particles.

$$\tau = \frac{\Delta V^t}{R_h} \eta$$

Where

- $\eta$  is the viscosity.
- $\Delta V^t$  is the tangential component of the relative velocity of the two spheres.

$$\Delta V^t = (V_1 - V_2) - ((V_1 - V_2) * n) * n$$

( $V_1$  and  $V_2$  are the velocities of the two spheres)

-  $R_h$  is the hydraulic radius defined as:

$$R_h = \frac{V_v}{S_s}$$

$V_v$  is the pore volume and  $S_s$  is the solid area of spheres in contact with fluid (figure 4.23).

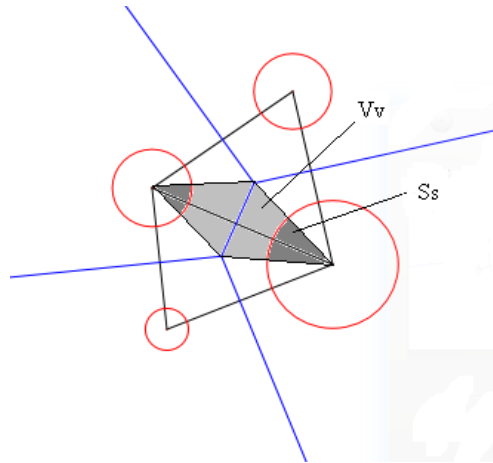


**Figure 4.24: pore volume and solid area of spheres.**

A simplified expression of the hydraulic radius was developed and used in the computation of the viscous force:

$$R_h = d + 0.45R$$

Where  $d$  is the interparticular distance and  $R$  is the mean radius of spheres.

#### **4.2.2. Determination of the interaction surface**

$S$  is the surface of interaction between two spheres (figure 4.24). It is defined as the area of the polygonal facet separating the spheres in the Voronoi's graph.

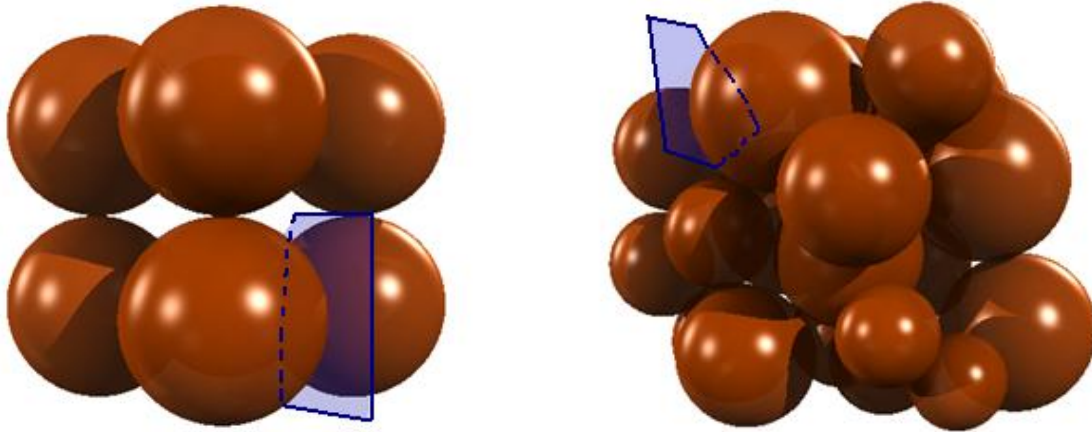


*Figure 4.25: Interaction surface in three dimensions.*

This area is the sum of triangles' area composing the polygon (figure 3.25).

The algorithm iterates on all triangles by incrementing vertices  $v_1$  and  $v_2$ .

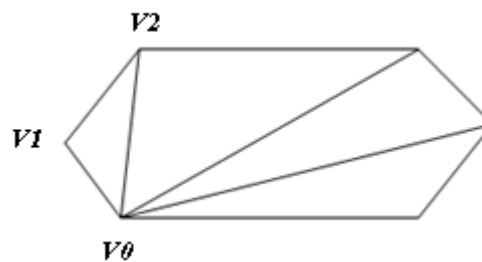


*Figure 3.26: interaction surface S.*

Vertices  $v_0$ ,  $v_1$  and  $v_2$  represent the centres of neighbouring tetrahedral cells to which the edge belongs.

The whole algorithm and functions corresponding to the computation of the shearing viscous force are coloured in blue in the code files presented in the appendix B.

### 4.3. Validation for a two sphere model

In order to verify our algorithm, we generate a model of 6 walls and two spheres of radius 0.2 m in contact.

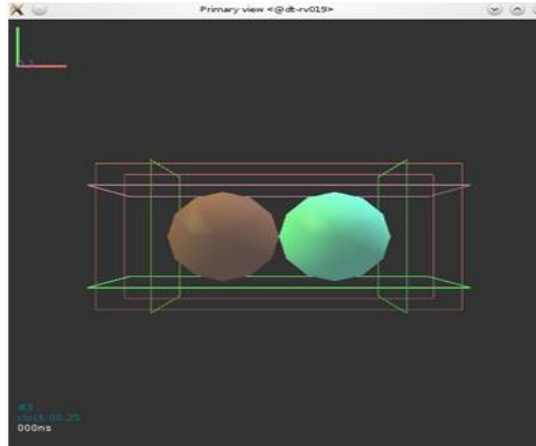


*Figure 3.27: the scheme of a two sphere model.*

The results of the area calculated by Yade are shown in table 2.

*Table 1: Interaction surface for the different edges:*

Body 1	Body 2	S (m <sup>2</sup> )
sphere 1	wall 3	0,16
sphere 1	wall 0	0,16
sphere 1	wall 2	0,16
sphere 1	wall 4	0,16
sphere 1	wall 5	0,16
sphere 2	Sphere 1	0,159
sphere 2	wall 2	0,16
sphere 2	wall 5	0,16
sphere 2	wall 1	0,16
sphere 2	wall 3	0,16
sphere 2	wall 4	0,16

If we compare these results to the analytical ones, we can confirm the adequacy of the method, because the interaction surface between two bodies (sphere and sphere or sphere and wall) is a square whose area is equal to  $4R^2 = 0.16 \text{ m}^2$  ( $R$  is the radius of the sphere).

Since the interaction surface is correct, we can check the shear stress expression defined by the equation ()

**Table 2: Shearing viscous force for a two spheres model:**

Body 1	Body 2	Viscous force (N)
sphere 1	wall 3	(0,0,0)
sphere 1	wall 0	(0,0,0)
sphere 1	wall 2	(0,0,0)
sphere 1	wall 4	(0,0,0)
sphere 1	wall 5	(0,0,0)
sphere 2	Sphere 1	(0,1.77,0)
sphere 2	wall 2	(0.00017,0,0)
sphere 2	wall 5	(0,1.77,0)
sphere 2	wall 1	(0,1.77,0)
sphere 2	wall 3	(0.00017,0,0)
sphere 2	wall 4	(0,1.77,0)

For all edges connecting a wall to the fixed sphere, the shearing viscous force is zero. When we talk about the edge connecting the two spheres (one is fixed and the other moves with a velocity  $U = (0, 1, 0)$ ), this force becomes equal to:

$$F = \frac{u - u_n}{R_h} * \eta * S = 1.77 \text{ N}$$

Where  $S = 0.16 \text{ m}^2$ ,  $R_h = 0.09 \text{ m}$  and  $\eta = 1$ .

The viscous shearing force has been validated for the simplest system of two spheres moving relatively.

We can now test our model in the more complex configuration of a set of spheres deposited in a shear flow under gravity.

#### 4.4. Application to a bed sediment subjected to a shearing flow

In order to study bed load transport, we prepare a sediment bed from an initial sedimentation of a suspension under the gravity effect in a quiescent fluid (figure 4.27). A constant velocity along the x direction is imposed as boundary condition on the top side of the domain. Particles begin to move under the influence of two factors: the gravity and a drag force exerted by the fluid on grains.

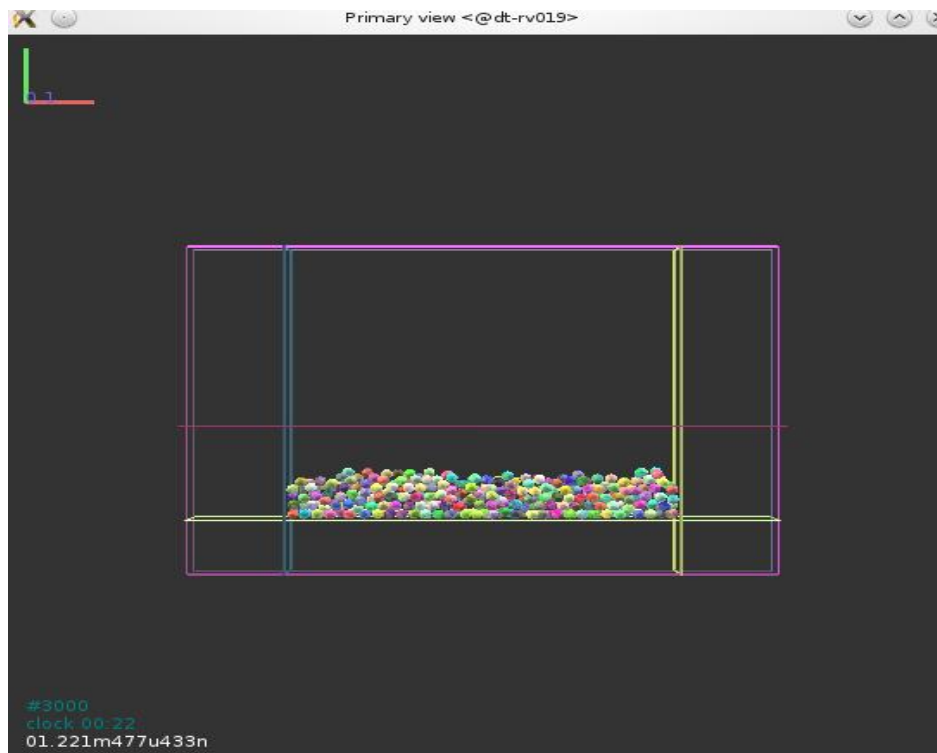


Figure 4.28: a bed load sediment model.

##### 4.4.1. Shields number

For low fluid velocity, particles don't move. There is so a threshold at which grains begin to be transported by the fluid. In 1936, Shields has introduced a dimensionless number that characterizes the motion threshold.

$$\theta = \frac{\tau}{(\rho_p - \rho_f)gd}$$

Where:

$d$  is the diameter of the grain.

$g$  the gravitational acceleration.

$\tau$  is the bed shear stress.

$\rho_p$  is the density of the particle.

$\rho_f$  is the density of the fluid.

It's the ratio between the hydro mechanical force or the drag force ( $\tau d^2$ ) and the apparent weight of a single particle ( $(\rho_p - \rho_f) g d^3$ ).

When the drag force tends to put grains in motion, the weight resists to this. The Shields number controls then the stability of the particles:

- $\theta < \theta_c$ : No motion.
- $\theta > \theta_c$ : particles are in motion.

$\theta_c$  is the critical Shields number from which particles start moving.

$$\theta_c = \frac{\tau_c}{(\rho_p - \rho_f)gd}$$

Experimental measurements show that the critical Shields number for the onset of particle motion is set to  $0.12 \pm 0.03$  for low Reynolds number. In the following simulations, he will be in the range  $10^{-1}$  -  $10^{-2}$ .

#### ***4.4.2. Evaluation of the critical Shields number***

In order to evaluate the critical Shields number, we impose a variable velocity on the top wall. As soon as particles begin to move, we calculate the viscous force applied on each grain and the corresponding Shields number.

The distribution of the Shields number is represented in figure 4.28. We can see that the mean critical Shields number is equal to 0.13 which is in agreement with the experimental results.

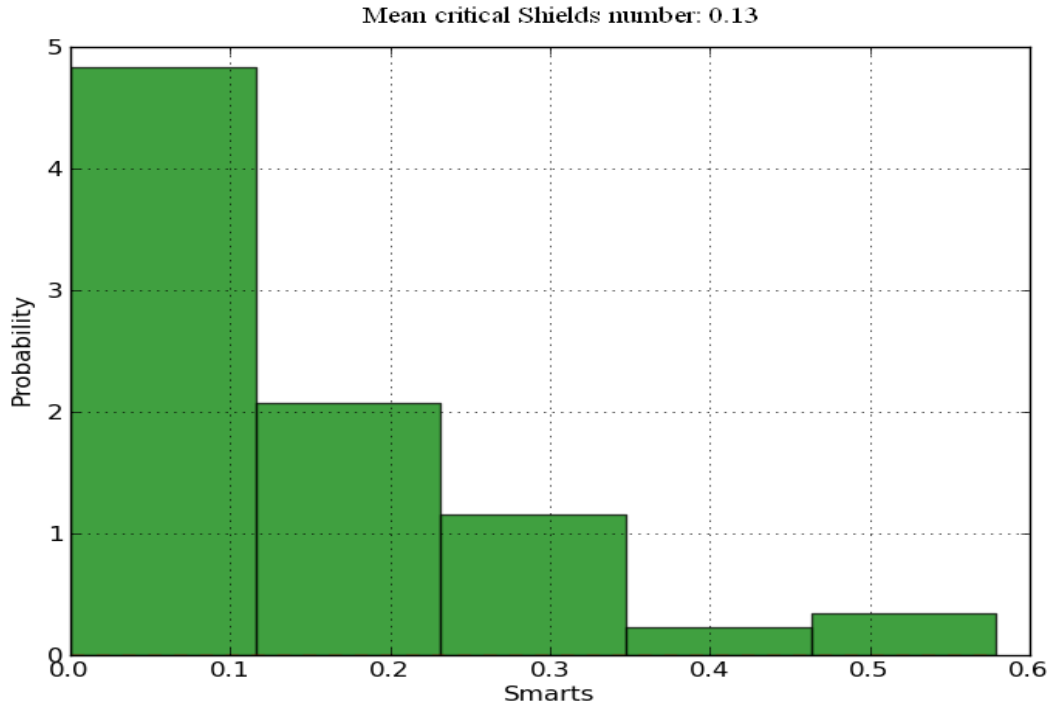


*Figure 4.29: Distribution of the Shields number corresponding to the onset of the grain motion*

If we look now to the evolution of the kinetic energy as a function of the viscous force, we set out the graph represented in the figure (4.29).

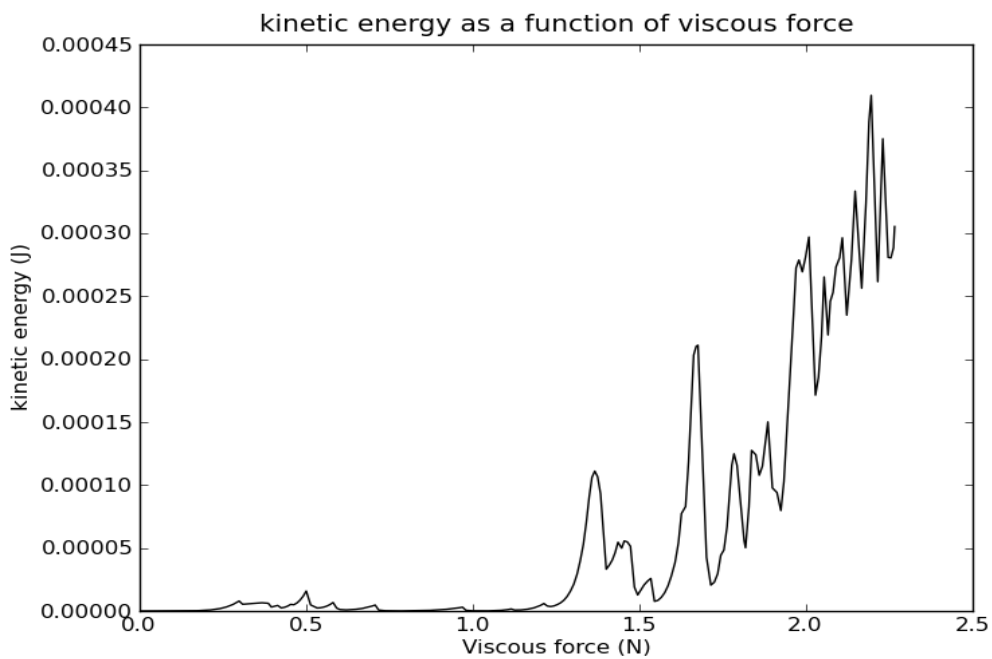


*Figure 4.30: Evolution of kinetic energy as a function of viscous force.*

Kinetic energy is very small (about  $10^{-8}$ ) for small values of viscous force; particles remain at rest. From a viscous force equal to about 1,3 N, kinetic energy increases and particles begin to move. This value of viscous force corresponds to a Shields number equal to 0,12.

#### ***4.5. Conclusion***

According to the DEM, we were able to study and control the motion of particles subjected to a shearing flow. We have validated the results obtained by experimental measurements by evaluating the critical Shields number. In fact, In a laminar flow, the onset of grain motion is characterised by a critical Shields number equal to  $0,12 \pm 0,03$  for small Reynolds number ( $Re < 1$ ).

## *Conclusions and perspectives*

The purpose of this work concerns the behaviour of immersed grains subjected to a shearing flow. This report has been divided into four main sections:

The first section recalled some basics of fluid mechanics and granular flow. It introduced to the Discrete Element Method which is a very efficient method for studying the different interactions in a granular material.

The second section presented the solid fluid coupling model developed in the 3SR lab and based on the Delaunay triangulation method. It was our starting point to study the shear behaviour of saturated granular materials.

Before starting our study of the shear in a granular material, we have begun in the third section with a simple model of Poiseuille flow where particles were fixed. We calculated the flow rate generated by Yade and compared it with the analytical results. Numerical and theoretical results are in agreement; the flow rate is independent of the geometric and mechanical properties of particles subjected to a Poiseuille flow, and depends only on the thickness of the gap between the two rigid blocks.

Finally, in the fourth section, we derive a model of viscous force in sheared granular materials, in the framework of Catalano's DEM-PFV model (original Catalano's model accounting only for volumetric deformations). This model has been implemented in Yade, then used to define the viscous shear forces exerted on particles in simulations of granular bed under tangential flow. The results have been analysed to determine the motion threshold defined by the so-called dimensionless Shields number  $\tau^*$ . The critical Shields number calculated numerically corresponds to the results given by experimental measurements: in a laminar flow, particles begin to be transported by the fluid for a critical Shields number equal to  $0,12 \pm 0,03$ .

As a conclusion, the DEM was a very promising method to study the behaviour of sheared saturated granular media. This method is becoming increasingly popular although it is relatively marginal compared to the Finite Element Method. This is because of the huge computational time it requires for large sized simulations, but results obtained with this method justify the effort it involves. We were able to elaborate and implement a model of viscous forces due to shear deformation, as a complement to Catalano's volumetric effects.

The study of rheology of an immersed granular material has been performed for an incompressible fluid through a totally saturated material and gave promising results. We didn't take into account the compressibility of the fluid however. For this reason, a PhD thesis is suggested in the 3S-R lab starting from the academic year 2011-2012 in which the tri-phased problems will be studied using the Discrete Element method, in the aim of developing a first and unique micro-hydro-mechanical coupling model in the three dimensional models.

## *References*

- [1] B.Chareyre, P.Villard; Dynamic Spar Elements and Discrete Element Methods in Two Dimensions for the Modeling of Soil-Inclusion Problems; J. Engrg. Mech. 131 (10 pages) – 2005.
- [2] V. Šmilauer, E. Catalano, B. Chareyre, S. Dorofeenko, J. Duriez, A. Gladky, J. Kozicki, C. Modenese, L. Scholtès, L. Sibille, J. Stránský, K. Thoeni, **Yade Documentation**. The Yade Project - 2010.
- [4] E. Guyon, J P. Hulin, L. Petit ; Hydrodynamique physique; EDP Sciences, CNRS éditions – 2001.
- [5] B. Chareyre ; Modélisation du comportement d’ouvrages composites sol-géosynthétique par éléments discrets, PhD Thesis Université de Grenoble I Joseph Fourier – 2003.
- [6] L. Sibille ; Modélisations discrètes de la rupture dans les milieux granulaires ; PhD Thesis, Institut National Polytechnique de Grenoble – 2006.
- [7] B. Chareyre, A. Cortis, E. Catalano, E. Barthélémy; Pore-scale modeling of viscous flow and induced forces in dense sphere packings; submitted, Transport in porous media - 2011.
- [8] V. Smilauer; Cohesive particle Model using the Discrete Element Method on the Yade Platform, PhD thesis - 2010.
- [9] PFC3D Manual; Contact constitutive models: theory and backgrounds (PFC3D)
- [10] D. Muller ; Techniques informatiques efficaces pour la simulation des milieux granulaires par des méthodes d’éléments distincts ; PhD thesis ; Ecole Polytechnique Fédérale de Lausanne – 1996.
- [11] Y. Forterre, O. Pouliquen; Flows of dense granular media – The annual review of fluid mechanics Vol. 40: 1-24 – 2008.
- [12] F. Chevoir, J N. Roux, F. Da Cruz, P. Rognon, G.Coval ; Lois de frottement dans les écoulements granulaires denses ; LMSGC Institut Navier.
- [13] J.-D.Boissonnat, O.Devillers, S.Pion, M.Teillaud, M.Yvinec. Triangulations in CGAL. Computational Geometry : Theory and Applications, 22:5-19, 2002.
- [14] O. Pouliquen ; Milieux granulaires ; CNRS Editions - 2001.
- [15] B. Andreotti, Y. Forterre , O. Pouliquen ; Les milieux granulaires, entre fluide et solide ; CNRS Editions – 2011.

[16] P.Cundall and O.Strack. A discrete numerical model for granular assemblies. *Géotechnique*, (29):47-65, 1979.

[17] ICG (2003), Pfc3d (particle flow code in 3d) theory and background manual, version 3.0. Itasca Consulting Group.